JB Accepted Manuscript Posted Online 27 September 2021
J Bacteriol doi:10.1128/JB.00407-21

1 **RESEARCH ARTICLE**

2

3 **Improved growth of *Escherichia coli* in aminoglycoside antibiotics by the *zor-orz* toxin-antitoxin**

4 **system**

5

6 Bikash Bogati[1], Nicholas Wadsworth[2], Francisco Barrera[2], Elizabeth M. Fozo[1*]

7

8 [1] Department of Microbiology, University of Tennessee, Knoxville, Tennessee

9 [2] Department of Biochemistry & Cellular and Molecular Biology, University of Tennessee, Knoxville,

10 Tennessee

11 [*]Corresponding author: Elizabeth M. Fozo, E-mail: efozo@utk.edu

12

13

14

ABSTRACT

Type I toxin-antitoxin systems consist of a small protein (under 60 amino acids) whose overproduction can result in cell growth stasis or death, and a small RNA that represses translation of the toxin mRNA. Despite their potential toxicity, type I toxin proteins are increasingly linked to improved survival of bacteria in stressful environments and antibiotic persistence. While the interaction of toxin mRNAs with their cognate antitoxin sRNAs in some systems are well characterized, additional translational control of many toxins and their biological roles are not well understood. Using an ectopic overexpression system, we show that the efficient translation of a chromosomally encoded type I toxin, ZorO, requires mRNA processing of its long 5' untranslated region (UTR; Δ28 UTR). The severity of ZorO induced toxicity on growth inhibition, membrane depolarization, and ATP depletion were significantly increased if expressed from the Δ28 UTR versus the full-length UTR. ZorO did not form large pores as evident via a liposomal leakage assay, *in vivo* morphological analyses, and measurement of ATP loss. Further, increasing the copy number of the entire *zor-orz* locus significantly improved growth of bacterial cells in the presence of kanamycin and increased the minimum inhibitory concentration against kanamycin and gentamycin; however, no such benefit was observed against other antibiotics. This supports a role for the *zor-orz* locus as a protective measure against specific stress agents and is likely not part of a general stress response mechanism. Combined, these data shed more insights into the possible native functions for type I toxin proteins.

IMPORTANCE

Bacterial species can harbor gene pairs known as type I toxin-antitoxin systems where one gene encodes a small protein that is toxic to the bacteria producing it and a second gene that encodes a small RNA antitoxin to prevent toxicity. While artificial overproduction of type I toxin proteins can lead to cell growth inhibition and cell lysis, the endogenous translation of type I toxins appears to be tightly regulated. Here, we show translational regulation controls production of the ZorO type I toxin and prevents subsequent negative effects on the cell. Further, we demonstrate a role for *zorO* and its cognate antitoxin in improved growth of *E. coli* in the presence of aminoglycoside antibiotics.

KEY WORDS: ZorO, type I toxin-antitoxin, *zor-orz*, aminoglycosides, *E. coli*, ATP, membrane proteins, antibiotic resistance

INTRODUCTION

Within the past two decades, numerous toxin-antitoxin (TA) systems have been identified encoded on bacterial chromosomes. A TA system consists of a relatively stable toxin which often targets an essential cellular function such as translation, DNA metabolism, energy production, or membrane homeostasis, and an antitoxin which counteracts the activity of its cognate toxin (1–4). Based on the nature of the antitoxin i.e., either a small RNA (sRNA) or a protein, and the mechanism used by the antitoxin to neutralize the toxin, a TA system is primarily classified into one of six types (type I – type VI) (4, 5). A type VII TA system has been proposed and an unorthodox TA system whereby an RNA is the toxin have recently been described, indicating further expansion of the variety of TA systems (6, 7). The toxin components of type I TA systems, which were first identified on plasmids, are small proteins usually under 60 amino acids (8, 9). In a type I system, the sRNA antitoxin neutralizes the toxin mRNA *via* complementary base pairing which in turn leads to degradation of the toxin mRNA, physical prevention of its translation, or both (4, 10). This repression in translation (in laboratory growth conditions) and the small size of the toxin protein makes the study of type I toxins difficult. Another challenge is that the deletion of one or even multiple TA gene pairs does not always produce an obvious phenotype (11–13). An ectopic overexpression system, therefore, is commonly used to investigate the interaction between the toxin and antitoxin and the impacts of the toxin protein on a bacterial cell.

ZorO is a type I toxin (29 amino acids) and one of the toxin components of the *zor-orz* locus. The *zor-orz* locus, first identified on the chromosome of *Escherichia coli* O157:H7 EDL933 (EDL933), encodes two highly homologous type I TA systems in tandem, *zorO-orzO* and *zorP-orzP* (*zorO* annotated as *z3289* and *zorP* as *z3290* in EDL933, GCA_000006665.1) (14, 15). Considering the *zorO-orzO* gene pair, *orzO* encodes a sRNA that specifically base pairs with the *zorO* mRNA, preventing translation and triggering its cleavage (14, 15). Increasing the amount of *zorO* mRNA *via* artificial overproduction from a plasmid allowed it to escape OrzO repression and cause cell stasis or death (14, 15). These toxic effects of ZorO may be due to its high hydrophobicity, similar to some other type I toxin proteins such as TisB (16),

HokB (17), and AapAI (18). Overproduction studies indicated an inner membrane localization of ZorO that leads to membrane depolarization and ATP depletion (19).

The secondary structures of many toxin-encoding mRNAs, including *zorO*, are either experimentally validated or predicted to inhibit their own translation by intramolecular sequestration of the ribosome binding sequence, providing an additional layer of toxin regulation (20). For those examined, processing of the untranslated region (UTR) of the mRNA is required for efficient translation. As an example, the full-length *tisB* mRNA is translationally inert and requires processing of the first 41 nucleotides of the 5' UTR for its translation (21). For the *zorO-orzO* gene pair, translation of the *zorO* mRNA is also repressed by a long 5' UTR (174 nucleotide), and the processed form (Δ28) was translated nearly 10-fold higher in an *in vitro* system (15, 22). Interestingly, for TisB, deletion of its antitoxin, *istR*, and the first 41 nucleotides of the mRNA which normally inhibit its translation, resulted in a strain with over 200-fold and 100-fold increase in the number of cells that survived lethal doses of ampicillin and ciprofloxacin respectively, as compared to the wildtype (23).

While ZorO overproduction is toxic, the role of the long 5' UTR in ZorO-induced cellular physiology has not been investigated. Herein, we show that the long 5' UTR of the *zorO* mRNA regulates its effects on translation *in vivo*, cellular growth inhibition, membrane depolarization, and ATP depletion in cells. In addition, we demonstrate the role of the *zor-orz* locus in improving growth in the presence of aminoglycoside antibiotics kanamycin and gentamicin. This is significant as improved growth and increased MIC (minimal inhibitory concentration) to specific antibiotics has not been attributed to a type I TA locus and indicates that the protective effects of a type I toxin may be towards specific stress agents.

RESULTS

ZorO translation and toxicity are dependent upon its 5'UTR. We previously demonstrated that overexpression of the *zorO* mRNA was toxic to *E. coli* when the mRNA was expressed from a multicopy plasmid behind the arabinose inducible promoter (P_{BAD}; 14, 15, 22). To confirm that this toxicity was due to the predicted encoded 29 amino acid protein ZorO, we mutated the start codon from an ATG to an

AAG. As shown in Fig. S1A, overexpression of the AAG mutant did not inhibit growth of *E. coli*, confirming the encoded protein is responsible for toxicity.

There are two dominant forms of the *zorO* mRNA: one possessing a 174 nucleotide (nt) 5' UTR (full-length) and a second, referred to as Δ28-*zorO*, lacking the first 28 nt of the 5' UTR as observed by primer extension assay and 5' rapid amplification of cDNA ends (5' RACE; Fig. S1B, S1C, (22)). The *zorO* mRNA levels upon artificial overproduction from these two different 5'UTRs under similar induction condition showed transcript levels equivalent to or even lower for Δ28-*zorO* as compared to the full-length 5' UTR (22). However, *in vitro* translation of the Δ28-*zorO* mRNA was more robust than that of *zorO* possessing its full-length 5' UTR (22). The contribution of processing in regards to ZorO-induced toxicity though was not previously examined. To address the significance of the UTR in ZorO-induced phenotypes, we cloned *zorO* with a C-terminus FLAG tag with either its full-length 5'UTR (P_{BAD}-*zorO*-FLAG) or its processed form (P_{BAD}-Δ28-*zorO*-FLAG), under control of an arabinose inducible promoter (P_{BAD}) on a high copy plasmid (Fig. 1A). The plasmids were transformed into a derivative of *E. coli* MG1655 (UTK007) that naturally lacks the *zor-orz* locus (14, 15). Induction of ZorO from either plasmid with high levels of arabinose, 13.32 mM (0.2%), resulted in an immediate growth stasis (Fig. 1B) and loss of viable cells (Fig. 1E). When induced with either 6.67 μM or 0.67 μM (0.0001% or 0.00001% respectively) arabinose, cells harboring P_{BAD}-Δ28-*zorO*-FLAG still resulted in nearly instantaneous growth stasis while those cells harboring P_{BAD}-*zorO*-FLAG were able to grow, although at a reduced rate to controls (Fig. 1C and 1D).

Considering the similar effects of P_{BAD}-*zorO*-FLAG and P_{BAD}-Δ28-*zorO*-FLAG on growth inhibition when induced with 13.32 mM arabinose (Fig. 1B), we used this induction condition to compare production of ZorO from the differing 5' UTRs. Using dot blot analysis, we were able to detect ZorO from both the full-length UTR and Δ28 UTR (Fig. 1F). However, using western blot analysis, we were able to detect ZorO-FLAG only when overproduced from the Δ28 UTR but not the full-length 5' UTR (Fig. S2A). In addition, we confirmed the inner membrane localization of ZorO via western blot analysis

after subcellular fractionation (Fig. S2B) as previously shown by Otsuka *et al*. (19). The cytoplasmic control Pgm was also observed in the inner membrane fraction, as was previously reported (24).

To further validate the translational effects were solely due to the differing 5' UTRs, we replaced the *zorO* coding sequence with that of green fluorescent protein (*gfp*) in a multicopy plasmid vector under control of the arabinose inducible promoter. *E. coli* cells harboring these plasmids with *gfp* under the two different *zorO* 5'UTRs were grown on LB agar with 13.32mM arabinose. When we examined colonies (2X magnification) for GFP production we observed green fluorescence only in the colonies expressing *gfp* under the processed 5'UTR (Δ28 UTR, Fig. S2C). Similarly, GFP detection via western blot analysis was greater from the processed 5' UTR as compared to the full-length UTR following induction with 13.32 mM arabinose for 30 min (Fig. S2D). When lower concentrations of arabinose (3.33 μM and 6.67 μM) were used to induce GFP production, we were only able to detect GFP from the Δ28 UTR and not the full-length 5'UTR (data not shown). Thus, the *zorO* UTR is sufficient to control translation of a heterologous mRNA.

ZorO forms an alpha helix across a lipid bilayer. Given the inner membrane localization of ZorO ((19), Fig. S2B), we determined the conformation that ZorO adopts in membranes. We used a reconstituted system to examine the structure of synthetic ZorO within lipid vesicles. To partially mimic the lipid composition of the *E. coli* inner membrane, we utilized vesicles composed of a 3 to 1 molar ratio of two lipids: 1,2-dioleoyl-sn-glycero-3-phosphoethanolamine (DOPE) and 1,2-dioleoyl-sn-glycero-3-phosphoglycerol (DOPG). We first used circular dichroism (CD) to study the conformation that ZorO adopts in the lipid bilayer. Fig. 2A shows a CD spectra with minima at 208 and 222 nm, which is characteristic of an α-helical conformation (25), indicating that ZorO folds into an α-helix. To discriminate if the helix lies on the surface of the membrane or if it is inserted across the lipid bilayer, forming a transmembrane helix, we employed oriented CD (OCD), which allows distinguishing between

155 these two possibilities. The OCD data shown in Fig. 2B indicate that ZorO forms a transmembrane helix,
156 given the single minima at 225 nm (26).
157
158 **Overexpression of *zorO* via its processed 5' UTR causes increased membrane depolarization and**
159 **ATP depletion**. The overproduction of ZorO, like other type I toxins including TisB (23, 27), DinQ (28),
160 HokB (1), IbsC, and ShoB (29), caused membrane depolarization (19). The data in Fig. S2B and the work
161 of others (19) indicated that ZorO targets the cytoplasmic membrane. However, we did note differences in
162 ZorO production (Fig. 1F, S2A) dependent upon whether it was expressed from the full-length or Δ28
163 UTR and wanted to further investigate how expression from the differing UTRs may influence ZorO-
164 induced physiology. We first assessed the differences in membrane depolarization using bis-(1,3-
165 dibtylbarbituric acid) trimethine oxonol dye ($DiBAC_4$-3) which is a potential-dependent distributional
166 fluorescent dye. This dye selectively enters cells upon membrane depolarization which are then measured
167 using a flow cytometer (30).
168 We used plasmids harboring *zorO* with differing lengths of its 5' UTR (full-length and Δ28 UTR
169 lacking FLAG tag). *E. coli* UTK007 cells transformed with these plasmids were induced with a final
170 arabinose concentration of 1.33 μM (0.00002%) and analyzed for membrane depolarization (Fig. S3), as
171 this arabinose concentration yielded growth inhibition of P_{BAD}-Δ28-*zorO* (Fig. S4B). Under this low level
172 of arabinose induction, membrane depolarization occurred within 15 minutes of ZorO overproduction
173 (Fig. 3A). We did observe that the percentage of cells positive for membrane depolarization was
174 significantly lower (**, $p<0.01$, ***, $p<0.001$) for those harboring the plasmid containing the full-length
175 5' UTR of *zorO* (~20%), as compared to the truncated (Δ28-*zorO*) UTR (~95%) (Fig. 3A, Fig. S3). When
176 the concentration of arabinose was raised to 3.33 μM (0.00005%, Fig. 3B) or higher (data not shown), the
177 impact on membrane depolarization was similar across all constructs examined with depolarization of
178 most cells (>95%) within 15 min of ZorO overproduction (Fig. 3B). It is important to note that despite
179 this severe impact on membrane depolarization when overproduced via the full-length 5'UTR, the

translated ZorO protein was below our detection limit using western blot analysis (Fig. S2A) even when induced with higher (13.32 mM) arabinose concentration.

Given the differences in membrane depolarization, we examined how the 5' UTR impacted ATP depletion using a quantitative luciferase-based assay (BacTiter-Glo™ Microbial Cell Viability Assay, Promega). In agreement with the membrane depolarization analyses, we observed that, at high levels of arabinose induction for 30 min, both 5'UTR variants depleted the ATP levels similarly (Fig. 3D). However, 15 min after addition of either 3.33 μM (0.00005%) or 6.6 μM (0.0001%) arabinose, overexpression of *zorO* from the Δ28-UTR significantly reduced cellular ATP levels as compared to the full-length 5' UTR (Fig. 3C).

ZorO induced damage is not due to gross morphological changes. Regardless as to whether its 5' UTR is processed or not, ZorO overproduction can still lead to severe membrane damage. The type I toxin protein HokB also causes membrane damage: it has been shown to insert in the cytoplasmic membrane and forms pores causing leakage of intracellular ATP (17, 31). We thus tested if ZorO formed large pores in the inner membrane that could result in ATP leakage. To enhance the overproduction of ZorO, we constructed the plasmid P_{BAD}-No-UTR-*zorO* by removing the 5'UTR and only leaving the ribosome binding site (Fig. S4A). The growth inhibition *via* this construct was similar to that of the P_{BAD}-Δ28-UTR-*zorO* (Fig. S4B). We then tested if leakage of ATP occurred when ZorO was overproduced by measuring extracellular ATP, but did not observe increased ATP levels in the supernatant compared to that of the cultures with empty vector (Fig. S5A). When cells carrying the empty vector were treated with butanol, a large amount of ATP was detected in the supernatant (Fig. S5A).

We further validated these findings using a reconstituted system to examine if ZorO-permeabilized membranes allowed the release of medium-sized organic molecules. To this end, we performed a leakage assay where the fluorescent dye calcein was encapsulated in lipid vesicles. Calcein has a molecular mass of 622.5 Da, similar to that of ATP (507.2 Da). We performed a titration experiment to determine if the

addition of ZorO would result in a release of calcein molecules. TritonX-100 was used to obtain total calcein release from the vesicles and the fluorescence corresponding to this sample was then used to normalize the fluorescence observed after addition of ZorO. We observed that the addition of ZorO resulted in no significant release of calcein molecules from the vesicles (Fig. S5B). These results indicate that ZorO does not cause a large disruption of the membrane integrity, as calcein did not exit the vesicle under the concentration range studied.

We also performed scanning electron microscopy (SEM) of cells overproducing ZorO (using P_{BAD}-No-UTR-*zorO*; Fig. S4A) to determine if the toxin caused any morphological alterations (Fig. 4). In contrast to the marked growth inhibition and cell death after ZorO overproduction, there were no overt differences in morphology (Fig. 4A) even when induced with a high concentration of arabinose (13.32 mM). Measurement of cell length (see Materials and Methods) revealed that ZorO induced cells were longer than uninduced cells (****, $p<0.0001$, Fig. 4B) but this was the only observable morphological difference.

Multiple copies of *zor-orz* locus contributes to survival in the presence of aminoglycosides. Virtually all antibiotics target active cellular processes, therefore active cellular metabolism is critical for effective killing by these drugs. ZorO overproduction caused membrane depolarization and reduced cellular ATP levels, which is expected to decrease metabolic activity. Reduced ATP levels in turn are linked to increased bacterial survival in the presence of antibiotics (1, 17, 32, 33). Further, type I toxins TisB and HokB are known to increase survival in the antibiotic ciprofloxacin or ofloxacin (1, 34, 35), thus, we investigated whether the *zor-orz* locus impacted cell growth and inhibition by antibiotics.

Given that ZorO overproduction is toxic, we first examined how increasing the copy number of the entire *zor-orz* locus would influence growth in the presence of antibiotics. To this end we cloned the entire *zor-orz* locus, including all transcriptional and translational control elements, into pBR322 (pBR-*zor-orz*) and examined the effects on antibiotic sensitivity in *E. coli* UTK007 (that naturally lacks the *zor-orz* locus) using a disc diffusion assay. Cells harboring *zor-orz* had statistically smaller zones of inhibition

upon exposure to the aminoglycoside kanamycin, a protein synthesis inhibitor, but not to ciprofloxacin (DNA gyrase inhibitor; Fig. S6). *E. coli* with multiple copies of *zor-orz* also had a higher minimum inhibitory concentration (MIC) to kanamycin and gentamicin but not to chloramphenicol or ciprofloxacin when grown in Mueller Hinton broth, the standard medium used in clinical laboratories (Table S3).

Given the increase in MIC, we then examined whether cells harboring multiple copies of the *zor-orz* locus could grow better in the presence of antibiotics than control cells. As *zorO* transcription may be sensitive to carbon source (data not shown), we investigated growth in rich media (LB) as well as minimal media with either glucose or fructose as a carbon source. Further, we utilized a microplate as opposed to glass tubes which were used for MIC determination (see Materials and Methods for details). We noted that cells harboring pBR-*zor-orz* grew far better in the presence of kanamycin in LB and also in M9 minimal media supplemented with 0.2% glucose, or 0.4% fructose (Fig. 5). Similar improved growth was observed with gentamycin (data not shown), but not with ciprofloxacin or chloramphenicol (Fig. S7).

To test the effect of multiple copies of the *zor-orz* locus in its native strain EDL933, we transformed these plasmids into an ELD933 strain in which we deleted the entire *zor-orz* locus (EDL933-Δ*zor-orz*). Similarly, there was improved growth of the cells harboring pBR-*zor-orz* plasmids in LB and minimal media (with glucose or fructose) in the presence of kanamycin (Fig. 6).

The uptake of kanamycin is dependent upon membrane potential and ATP (36). As artificial overproduction of ZorO can result in ATP depletion (Fig. 3), we wanted to determine if cells harboring multiple copies of the *zor-orz* locus had a reduced ATP levels. To test this, we grew EDL933-Δ*zor-orz* transformed with either pBR or pBR-*zor-orz* in LB until mid-log phase, split the culture, and treated half the culture as mock or added 4 µg/ml of kanamycin to the other half to better monitor the immediate cellular response to kanamycin. This also eliminated differences in the growth patterns observed above (Fig. 6). For our mock-treated cultures, the relative ATP levels were similar regardless of whether the strain harbored either the empty vector (pBR) or pBR-*zor-orz* (Fig. S8A). For those cells treated with kanamycin, we observed no differences in relative ATP levels after 1 hour (hr) of treatment, but saw

relatively lower ATP levels in cells harboring pBR-*zor-orz* following 4 hrs of kanamycin treatment (*, $p < 0.05$, Fig. S8B). We also analyzed the effect on membrane depolarization upon treatment with kanamycin. There was no statistically significant difference in the percentage of cells with a depolarized membrane, but those cells harboring pBR-*zor-orz* did trend lower (i.e., fewer cells positive for depolarization) 1 hr post kanamycin treatment (Fig. S8C). We observed improved growth, however, of cells harboring pBR-*zor-orz* compared to those harboring the empty vector only approximately 5-6 hrs after kanamycin addition (Fig. S8D).

To further test if this improved growth of *E. coli* cells in the presence of aminoglycoside antibiotics is maintained at a single copy level, *i.e.*, chromosomal level, we generated a derivative of *E. coli* MG1655 (which naturally lacks the *zor-orz* locus) in which we integrated into the genome a single-copy of *zorO* under control of its processed UTR (Δ28) and native promoter (this strain lacks the OrzO antitoxin). Unlike the effects observed with multiple copies of the *zor-orz* locus, the single copy of *zorO* integrated in the *E. coli* chromosome was unable to improve growth in the presence of kanamycin or gentamycin (Fig. 7B and 7C). We also constructed a similar EDL933 strain (EDL933-Δ28-*zorO*) and compared its growth with the WT and the EDL933-Δ*zor-orz*. The growth patterns of the EDL933 strains were similar in LB (Fig. 7D) and M9 minimal media supplemented with glucose or fructose (data not shown). Like the above observations of our derived MG1655 *E. coli* strains, there was no significant differences in the growth pattern of these three EDL933 strains in the presence of kanamycin (Fig. 7E), gentamicin (Fig. 7F), chloramphenicol, or ciprofloxacin (data not shown).

DISCUSSION

In this study, we demonstrated that the physiological consequences of ZorO production in *E. coli* are directly regulated by the length of its 5' UTR. Previously, we characterized two forms of the *zorO* 5' UTR: a full-length (174 nt) that is prominent and a Δ28 form, that is the result of processing of the 5' end by an unknown ribonuclease (Fig. S1B and S1C, (22)). Herein, we demonstrated that overproduction of

281 Δ28-*zorO* led to greater cell death, faster and more severe membrane depolarization, and ATP depletion.
282 However, analyses of dye and ATP leakage, together with a lack of morphological changes, support that
283 ZorO does not form large membrane pores, but instead, likely causes cellular death by forming small,
284 possibly selective pores, resulting in ion imbalance preventing ATP production. An increase in the copy
285 number of the entire *zor-orz* locus allowed for improved growth and increased MIC in the presence of
286 aminoglycoside antibiotics without the complicating effects of the natural toxicity of ZorO
287 overproduction.
288
289 *Role of 5'UTR in subsequent effects of ZorO toxin protein.* Unlike other TA systems, in which the two
290 genes are transcribed from the same promoter, to date all identified type I TA genes are transcribed from
291 their own promoters (20, 37) making it more challenging to balance the TA ratio. However, for those type
292 I toxins that have been studied in depth, most possess extensive 5' or 3' UTRs that often play a role in
293 translational regulation (20). The 3' processing of the *hokB* mRNA results in major structural
294 rearrangements in the 5'-end, resulting in translational activation or inactivation via sRNA binding (38).
295 Similarly, the *aapA1* toxin mRNA in *Helicobacter pylori* has also been shown to undergo 3' end
296 processing via the 3'-5' endonuclease activity of the polynucleotide phosphorylase (39).
297 The control of ZorO translation *via* processing is most similar to *tisB*. In this case, the full-length
298 *tisB* mRNA was not translated when using an *in vitro* system, but the processed form, referred to as Δ41
299 *tisB*, was translated readily and overproduction of this variant was far more toxic (21, 23, 40). However,
300 unlike *tisB*, the *zorO* full-length mRNA could be translated using an *in vitro* system, though not nearly as
301 robustly as Δ28 (22). Whether or not the differences in the ability to translate the two toxins from their
302 respective full-length 5' UTRs *in vitro* mirrors what occurs in an *E. coli* cell is not clear. The ribosome
303 binding site (RBS) of both *tisB* and *zorO* are occluded in stem structures, preventing ribosomes from
304 interacting. For *tisB*, processing allows for the interaction of ribosomal protein S1 with the standby site
305 (upstream of the true RBS) of the mRNA; this is thought to stimulate structural unwinding, opening of the

sequestered RBS, and eventually, binding of the ribosome to the RBS (40). While this mechanism has not been demonstrated for *zorO*, the similarities in structural requirements for translation suggest that the stand-by site model is likely true (22). Interestingly, *dinQ* and *shoB* also undergo a 5'-end processing, which might be regulated similarly to prevent toxin translation (28, 41).

The combination of our current work and past findings (22) supports the significance of the UTR for proper regulation of *zorO* given the potential detrimental effects of excess ZorO on cells. Further, previous and current work suggests that only a portion of the total mRNA population is subject to processing (Fig. S1, (22)) and this likely leads to uneven production of ZorO across the population. Our physiological data support this as well: there is a clear delay in membrane depolarization and ATP depletion for cells overproducing ZorO under the full-length 5' UTR versus the processed form (Δ28, Fig. 3). This may help in "bet hedging" by having only a portion of the population reduced in growth from ZorO overproduction while positioning the population as a whole to deal with a sudden stressor that cells with higher metabolic activity would be more susceptible to. It may also be that cells accumulate full-length *zorO* mRNA that is not processed but then a processing event (note that the enzyme responsible for such processing is unknown) can be triggered by environmental stressors. In this manner as well, each cell may "bet-hedge" by accumulating the toxin mRNA to be poised for changing conditions.

ZorO: a membrane targeting toxin. The hydrophobic nature of the ZorO protein suggested it could be a membrane protein which was later confirmed to localize to the inner membrane (Fig. S2B, (19)). Reconstitution experiments showed that ZorO does not damage the integrity of the membrane bilayer (Fig. S5B). These results agree with the SEM data which did not show membrane damage or large morphological disruptions upon ZorO production (Fig. 4). Additional experiments in lipid vesicles showed that ZorO adopts a helical conformation. The magnitude of the helical signal is comparable to other peptides of similar size that adopt a TM topology (42–44). Finally, OCD experiments established that ZorO inserts into a TM configuration with a helical orientation close to perpendicular to the

membrane plane (Fig. 2). This result agrees with the lack of gross membrane disruption and if ZorO indeed forms an ion channel, our data would support a closely tightened TM bundle.

Although many type I toxins are predicted to target and damage the membrane, only a handful of them have been experimentally verified (16–18, 45, 46). Apart from the membrane, some type I toxins target nucleic acid (47, 48) or cell envelope biosynthesis (49). It is currently unclear why some hydrophobic toxins appear to readily target the membrane while others impact different cellular processes. When expressed at endogenous levels, these toxins may interact with specific cellular proteins. This, however, has not been examined to the best of our knowledge.

Effects of toxin protein on bacterial morphology. The AapA1 toxin in *Helicobacter pylori* triggers a massive and rapid morphological transformation of this spiral-shaped bacterium into round coccoid cells (46). Additionally, HokB has been implicated in ghost cell formation (50), and Fst results in filamentous cells with multiple invaginations affecting cell division with no obvious pores or loss of intracellular material (47). ZorO overproduction decreases membrane potential and cellular ATP levels, however, it does not cause immediate cell lysis based on microscopy (Fig. 4) and absence of cell debris (laboratory observation). A marked reduction in the colony forming units though was seen as soon as 15 minutes after induction (22). These differences in cell morphology caused by the type I toxin proteins may be due to differing overproduction levels. However, it likely also implies differences in the nature of the toxin properties, *i.e.*, the direct target of the toxin. For example, Fst overproduction leads to near immediate condensation of DNA (51). This would greatly impact DNA replication and cellular division, which would be reflective in the observed morphology (52). If ZorO does self-oligomerize in the membrane, the resultant channel formed would be narrow (see above), likely allowing only ion permeation, and would not leak organic molecules or cause morphological alterations. This in turn would explain both the lack of gross morphological changes and visible cellular debris upon ZorO overproduction.

356 *The zor-orz locus: a type I TA system with specificity against aminoglycoside antibiotics.* A role of the
357 type I toxin proteins TisB and HokB has been established in bacterial persistence as a result of membrane
358 depolarization and ATP reduction (1, 17, 23, 35). Persister cells are a subpopulation within a bacterial
359 culture that can survive a high dose of antibiotics but are not genetically resistant (i.e., they cannot grow
360 in the presence of the tested antibiotic). Increases in the persister population when cells were treated with
361 ofloxacin (targets DNA gyrase) and tobramycin (aminoglycoside, targets ribosome) have been observed
362 with HokB (1). TisB production can also increase the number of persister cells when treated with
363 ciprofloxacin (targets DNA gyrase), ampicillin (targets cell wall), and streptomycin (protein synthesis
364 inhibitor) (1, 23, 35). This suggests a broader range of protection from their production. We tested for the
365 level of persister cells in EDL933 *Δzor-orz* locus against ciprofloxacin and ampicillin and did not see
366 significant difference comparted to the parental strain (data not shown). However, as shown in this study,
367 increasing the copy number of the *zor-orz* locus (while avoiding its toxicity) improved growth in presence
368 of aminoglycosides but not other antibiotics examined. We also observed an increase in MIC against
369 kanamycin and gentamycin (Table S3). Overproduction of some *de novo* synthesized small membrane
370 proteins has been shown to increase MIC against aminoglycosides (53); however, to our knowledge this
371 is the first report of a type I TA system conferring an increase in MIC.

372 Why is there such specificity for aminoglycosides? A model for ZorO function, as noted earlier, is
373 the possible formation of small oligomers (either dimers or multiple dimers) that lead to ion flux. Similar
374 to that of TisB (54), ZorO is hypothesized to form an antiparallel dimer within the membrane. The "non-
375 specific" metabolic effect of ZorO does not broadly protect from antibiotic classes other than
376 aminoglycosides while both TisB and ZorO lead to membrane depolarization and ATP depletion (Fig. 3)
377 (16, 19). Aminoglycoside uptake occurs in three stages where the latter two are dependent on membrane
378 potential and ATP (55). Therefore, membrane depolarization and decreased ATP levels can reduce the
379 uptake of aminoglycosides. However, our data demonstrated no basal differences in the percentage of
380 depolarized cells for cells harboring empty plasmid versus pBR-*zor-orz* when grown in LB (Fig. S8CA).
381 Even upon treatment with kanamycin, there were no changes in ATP levels within the first hour of

treatment (Fig. S8B). This suggests that *zor-orz* has an alternative mechanism for allowing growth in kanamycin. Similarly, additional studies have shown that while small alpha helical peptides that reduce membrane potential can be protective against aminoglycosides, not just any transmembrane helix can, including other type I toxin proteins (53). These data indicate that not all type I toxins behave similarly and that there is likely specificity in their targets and effects on cellular physiology.

The chromosomal copy of *zorO* without its two known translational repressive elements i.e., full-length UTR and the OrzO sRNA, however, did not show a difference in growth in LB, LB with kanamycin, or LB with gentamicin as compared to the wild type MG1655 *E. coli* strain in the presence of kanamycin and gentamycin (Fig. 7A, 7B, and 7C). This result was consistent with the EDL933 strains tested (Fig. 7D, 7E and 7F). A similar strain of *E. coli* in which the two translational repressive elements of the toxin *tisB* were removed did result in an increase in the number of persistent cells that survived lethal doses of ampicillin and ciprofloxacin respectively (23). So, why is there a lack of phenotype for ZorO production from the chromosome in absence of the regulation by antitoxin OrzO and 5'UTR? It is possible there may be other yet to be identified regulatory elements that prevent ZorO induced effects and its function at chromosomal level under the conditions used in this study. Further, it is possible that under endogenous production, ZorO (and other type I toxins) may interact with specific protein partner(s) to modulate activity and a lack of observable phenotype may be because levels of ZorO are not high enough under the conditions examined to observe differences across a population of cells.

Is ZorO really a toxin? While ectopic overproduction of ZorO results in a quick cell growth stasis, multiple copies of the *zor-orz* locus with its native regulatory elements do not impact growth of cells in LB or minimal media supplemented with glucose or fructose (Fig. 5). Similarly, a single copy of *zorO* (with a processed 5'UTR) on the chromosome of either MG1655 or EDL933 also showed no impact on growth in LB (Fig. 7) or minimal media (data not shown). Reports for other type I toxins TisB (23) and TimP (12) also demonstrated a lack of growth effects in rich medium such as LB when expressed from

the chromosome. Questions thus remain as to when some chromosomally encoded toxins are active and if they truly can induce cell stasis or death when expressed at the endogenous level.

Overall, our data indicate that the 5'UTR of *zorO* plays a vital role in regulating the translation and subsequent cellular impact of the small toxin protein ZorO. Overexpression from the processed 5'UTR significantly impacts membrane depolarization and ATP depletion in the cells without causing a major change in bacterial morphology. Cells harboring multiple copies of the *zor-orz* locus, under control of its native regulatory elements, are not broadly protected against stress but do have increased resistance to aminoglycosides. These results, combined with data from other type I toxins, suggest that type I toxin proteins have unique effects on bacterial cells.

EXPERIMENTAL PROCEDURES

Strains, plasmids, and culture conditions. The strains and plasmids used in this study are listed in Supplemental Table S1. The sequences of all oligonucleotides are listed in Supplemental Table S2.

Growth conditions. Cultures for overproduction of ZorO were grown as described previously (15). Briefly, *E. coli* UTK007, a derivative of MG1655 with constitutive *araE*, was transformed fresh (not older than 10 days) with the indicated plasmid derivatives of pAZ3 using either electroporation or chemical transformation (15). The resulting transformants were grown overnight in 5 mL LB (with 25 μg/ml chloramphenicol final concentration) at 37^{o}C with shaking and diluted in LB with chloramphenicol to an OD_{600} of 0.01. When the OD_{600} reached ~ 0.3, arabinose was added to a final concentration of 13.32 mM (0.2%), 6.67 μM (0.0001%), 3.33 μM (0.00005%), 1.33μM (0.00002%), or 0.67 μM (0.00001%) as indicated in the text. *E. coli* UTK007 carrying empty vector (pAZ3) or uninduced (no arabinose) was used as a control. OD_{600} was measured as shown in the figures and cells were harvested at indicated time points after overexpression. Shown are averages ± standard deviations for a minimum of three replicates.

Microplate growth curves. Overnight cultures were grown either in LB medium or M9 (1X M9 salts, 2mM $MgSO_4$, 0.1mM $CaCl_2$, 1μg/mL thiamine, supplemented with carbon source as indicated). Ampicillin (100 μg/ml final concentration) was added when testing cells transformed with pBR322 (56) or pBR-*zor-orz* plasmids. Overnight cultures were diluted to an OD_{600} of 0.2 in 1 mL 1X sterile phosphate buffer saline (PBS) or sterile growth medium. A 96 well microplate was prepared by adding 190μl of the culture media (LB or M9) containing the antibiotics as indicated. Then 10 μl of 0.2 OD_{600} culture (diluted in PBS from overnight culture) was added to obtain a 200 μl total volume of a 0.01 OD_{600} culture. Absorbance was recorded on a Gen5^{TM} Microplate reader (BioTek Instruments, Inc.) every 30 min after a 15 sec of shaking for 24 hrs at 37^{o}C. Shown are averages ± standard deviations for a minimum of three replicates. Note, as we observed variation even in control strains emerging from lag phase when grown in M9 minimal media with fructose, we used 0.4% fructose as the final concentration.

Plasmid and strain construction. The overexpression plasmid P_{BAD}-*zorO*-FLAG (full-length 5'UTR) was generated by amplifying C-terminal FLAG tagged *zorO* using the oligonucleotides EF1065 and EF1279 from the EDL933 genome. To generate P_{BAD}-Δ28-*zorO*-FLAG, the insert was amplified with oligonucleotides EF1141 and EF1279 from the plasmid P_{BAD}-*zorO*-FLAG. To construct P_{BAD}-No-UTR-*zorO* (Fig. S4A), the insert was amplified from *E. coli* O157:H7 EDL933 genomic DNA with oligonucleotides EF1066 and EF1611.The N-terminus FLAG tagged *zorO* (with 5'UTR similar to that of P_{BAD}-No-UTR-*zorO*) was constructed by amplifying the insert with oligonucleotides EF1465 and EF1066. The inserts were digested and ligated into the EcoRI and HindIII sites of the high-copy plasmid pAZ3 (29) under control of the P_{BAD} promoter. To generate P_{BAD}-*zorO*-AAG, site directed mutagenesis (15) was performed on the plasmid P_{BAD}-*zorO* (22) using primers EF1325 and EF1326.

The plasmid pBR-*zor-orz* (with native regulatory elements) was constructed by amplifying the insert from EDL933 genomic DNA with oligonucleotides EF910 and EF 912, restriction digested and ligated into the HindIII and BamHI sites of medium copy pBR322 plasmid. The plasmid pBR-*zorO* was

456 constructed by amplifying the pBR-*zorO-orzO* plasmid using oligonucleotides EF1869A and 1870A (to
457 remove *orzO*) and was assembled using NEB Gibson Assembly Master Mix.
458 *E. coli* MG1655 UTK102 was derived from MG1655 UTK007 (15). P1 transduction was used to
459 replace the *lepB* with SPA (sequential peptide affinity) and kanamycin tagged version of *lepB* (inner
460 membrane localization control) (57). The kanamycin resistance gene (flanked by FRT sites) was removed
461 using pCP20 (58) and confirmed via PCR to generate UTK102. *E. coli*. MG1655 UTK105 was
462 subsequently derived from *E. coli* MG1655 UTK102 to replace *pgm* with a SPA tagged *pgm* (cytoplasmic
463 localization control) and confirmed via PCR.
464 To construct *E. coli* MG1655-Δ28-*zorO*, Δ28-FLAG-*zorO* linked to a chloramphenicol cassette
465 (flanked with FRT sites), inserts were amplified from a pBR322 plasmid construct using the
466 oligonucleotides EF1572 and EF1573 (Supplemental Table S2). The amplified insert was recombineered
467 into *E. coli* NM1100 utilizing the mini-λ-Red recombination system (59, 60). This was then moved into
468 *E. coli* MG1655 using P1 transduction. The antibiotic cassette was removed using pCP20 (58, 61). The
469 strain was verified via sequencing of the genetic region.
470 EDL933-Δ28-*zorO* was constructed by amplifying Δ28-FLAG-*zorO*-Kan using the oligonucleotides
471 EF1572 and EF1573 (Supplemental Table S2) from a plasmid vector that was synthesized (Genescript).
472 The amplified product was recombineered in EDL933, replacing the *zor-orz* locus as described previously
473 (59). The kanamycin resistant gene was then replaced with a chloramphenicol resistance gene amplified
474 from pKD3 using primers EF1795 and EF1796 (Supplemental Table S2). The chloramphenicol marker
475 was then removed via pCP20 treatment (61). The strain was PCR screened and confirmed via sequencing
476 of the genetic region.

477 Strain EDL933-Δ*zor-orz* was generated via recombineering as outlined previously using primers
478 EF585 and EF645 (Supplemental Table S2; (59)). The *zor-orz* locus was replaced with a chloramphenicol
479 resistance marker (flanked with FRT sites). The chloramphenicol marker was then removed via pCP20
480 treatment (61).

RNA isolation. *E. coli* cells harboring pAZ3-*zorO* were grown to $OD_{600} \approx 0.2–0.3$ and arabinose (13.32 mM) was added (time 0). Cells were harvested 15 and 30 min post-arabinose induction. For cells harboring pBR-*zorO*, *E. coli* was grown to OD 600 of ~0.3 and cells were harvested. Total RNA for all conditions was isolated via direct lysis as described previously (62).

Primer extension assay. Total RNA (5 μg) was isolated 30 min after arabinose induction (in LB medium) and was separated on a denatured 8% polyacrylamide-urea gel. Primer extension was performed as described previously using labeled primer EF524 (Supplemental Table S2; (14, 63)).

5' RACE analysis. 5' rapid amplification of cDNA ends (RACE) assay was performed as described previously (29). Isolated RNA was ligated to the RNA adapter A1. Reverse transcription was carried out with *zorO* 5' UTR specific primer EF510. Amplification of *zorO* cDNA was performed with Taq DNA polymerase and primers EF510 and A4. Amplified cDNA fragments were cloned into pCR®4-TOPO® vector (Invitrogen) and then sequenced.

Cell survival after ZorO overproduction. Cellular aliquots of 100 μl were collected at mid-log (OD600 ~0.3, before arabinose induction) and 1h post-arabinose induction. The aliquots were serially diluted in 900 μl of sterile 1X PBS of which100 μl was plated onto LB medium (with 25μg/ml chloramphenicol). The plates were incubated at 37^0C for 18-24 hrs and the colony forming units were counted. The log ratio of survivors was calculated by comparing the CFUs obtained after 1h arabinose induction to that before induction.

Western blot and dot-blot analysis. Total protein was extracted from a 50 ml culture (after overexpression for 30 minutes as indicated in the text) via bead beating. Protein concentration was measured using a Bradford Protein Assay. Protein samples (20μg) were separated on a NuPAGE Bis-Tris gel, transferred to the immobilon-FL membrane, and probed with a rat derived α-FLAG tag primary antibody and an α-IgG secondary antibody (LI-COR Biosciences) that fluoresces at 680 nm. LepB was tagged with SPA tag (UTK102) to serve as a loading control. For GFP detection, blots were probed with a

rabbit derived anti-GFP primary antibody (Invitrogen) and an α-IgG secondary antibody (LI-COR Biosciences) that fluoresces at 800 nm.

Subcellular fractionation was performed as described previously with modifications (57). Total protein lysate was ultracentrifuged (100,000 g, 4°C, 45 min) to yield supernatant (cytoplasmic proteins) and a pellet (membrane proteins). For separation of inner and outer membrane proteins, the pellet was washed with 1X PBS and resuspended in 500µl of 0.5% sodium-lauryl sarcosinate, incubated at room temperature for 30 min, and ultracentrifuged (100,000 g, 4°C, 15 min). The supernatant and pellet corresponded to the inner and outer membrane fractions respectively. Then inner membrane fraction was transferred and acetone precipitated while the pellet was washed with 0.5% sodium-lauryl sarcosinate and then resuspended in 1X PBS.

Protein samples (20µg) were loaded onto Novex 10-20% Tricine gels and transferred to an immobilon-FL membrane. Blots were probed with α-FLAG (BioLegend) and α-OmpA primary antibodies (Antibody Research Corporation) and α-IgG secondary antibodies (LI-COR Biosciences) fluorescing at 680 nm and 800 nm respectively.

Dot blots were performed by spot inoculating a nitrocellulose membrane with 10µl of the sample containing 10µg or 20µg protein and processing the membrane as above (probed with α-FLAG primary antibody α-IgG secondary antibody) (64).

Microscopic image of colonies expressing GFP under different 5' UTR variants. Overnight cultures of UTK007 cells transformed with either pAZ3-*zorO*-UTR-*gfp* or pAZ3-Δ28-UTR-*gfp* were serially diluted and plated on LB with 25 µg/ml chloramphenicol and 13.32 mM arabinose. Plates with 30-300 colonies were used to image under all-in-one fluorescence microscope BZ-X710 using bright field and green fluorescent channel with 2X magnification.

Membrane depolarization assay. Membrane potential sensitive dye Bis-(1,3-dibtylbarbituric acid) trimethine oxonol ($DiBAC_4$-3; InvitrogenTM) was used to determine the effect of ZorO production on membrane depolarization. A 25 mg/mL stock solution was prepared in dimethyl sulfoxide. At indicated time points, 50-100 µl of culture was taken, flooded with 4ml 1X PBS and centrifuged for 10 min at 4°C. Cells were resuspended in 1 ml PBS and stained with $DiBAC_4$-3 (10 µg/ml final concentration) for 20 min in the dark. After two steps of washing with 1X PBS, cells were re-suspended in 0.5 ml of PBS and analyzed by flow cytometry in an LSR II flow cytometer (Becton Dickinson) with a 488-nm laser. Samples were run at ~3000 events per second and fluorescence was collected in the fluorescein isothiocyanate (FITC) channel. Data was analyzed using FlowJo software package (FlowJo LLC, Ashland, OR, USA) such that the cells showing at least 10^3 abu or more fluorescence were gated and mean fluorescence intensity was obtained. All tests were done with a minimum of three biological replicates.

ATP measurements. ATP levels were measured using BacTiter Glo ATP Assay System Bioluminescence Detection Kit for ATP Measurement (Promega) according to the manufacturer's instructions. The observed relative luciferase unit (RLU) values were normalized to the OD_{600} at the time of cell harvest. A minimum of three biological replicates were performed per strain/condition. To determine ATP leakage, ATP measurements of the spent medium were determined. Cells were pelleted at indicated time points after ZorO overproduction and 100µl of the supernatant was used to measure the ATP concentration. As a control, cells carrying empty vector were treated with 5% (final concentration) of butanol for 5 min and ATP measurements of the spent medium were determined as above.

Circular dichroism (CD). The ZorO peptide was synthesized using Fmoc chemistry by ThermoFisher. The peptide sample had a purity of >95%, as assessed via HPLC. Peptide identity was determined by MALDI-TOF. Chloroform stocks of the synthetic lipids DOPE and DOPG (Avanti Polar Lipids) were dried and resuspended with a methanol solution of ZorO. The resulting solution was dried first with a stream of Argon, followed by overnight incubation under vacuum. Large unilamellar vesicles containing

552 ZorO reconstituted in the lipid bilayer were formed by extrusion. Standard and oriented CD experiments
553 were performed as described previously (65, 66).

554 **Membrane leakage experiments in vesicles.** Leakage experiments were performed after encapsulation
555 of calcein as described elsewhere (42). ZorO was added from methanol stocks at a 1% v/v final
556 concentration of methanol. No methanol induced leakage was observed. 1% (v/v) Triton X-100 was
557 added to the sample to obtain total calcein release and the fluorescence corresponding to this sample was
558 used for normalization.

559 **Scanning Electron Microscopy (SEM).** Cells harboring either empty vector pAZ3 or P_{BAD}-No-UTR-
560 *zorO* were grown in LB until mid-log phase (OD_{600} of ~0.3) and induced by adding 13.32 mM final
561 concentration of arabinose. At 30 min post-induction, cells were harvested (50 ml) and washed twice with
562 1x PBS to remove media. Fixation was performed with glutaraldehyde (3% final concentration) for 1h.
563 Cells were washed twice with distilled water and stored in 500µl of 1X PBS at 4^{o}C overnight. The next
564 day, samples were centrifuged, the supernatant was discarded, and 20µl of the pellet was transferred to
565 silicon chip with poly-L-lysine. The cells were dehydrated by immersion of the silicon chip in an
566 increasing concentration of ethanol (25%, 50%, 70%, 95% and 100 %) for 10 min each followed by a
567 critical point dry. The silicon chips were mounted to an aluminum mount, coated with iridium, and
568 observed under an Auriga Scanning Electron Microscope in Advanced Microscopy and Imaging Center,
569 University of Tennessee, Knoxville. Images from at least five random microscopic fields were taken at
570 5,000X and 20,000X magnification. The cells producing ZorO were analyzed for differences in
571 morphological characteristics as compared to the uninduced controls. Cell length was measured using
572 ImageJ (67). Cells (at least 30 per image) from each of the three biological replicates were analyzed.

573 **MIC determination**. Minimum inhibitory concentration was performed as previously described (68)
574 with slight modification. An overnight culture was diluted in Mueller Hinton Broth to 0.01 OD_{600} (with
575 100 µg/ml final concentration of ampicillin to maintain pBR plasmids). To a set of 10 sterile tubes, 1 mL

of the diluted culture was added to 8 tubes; to the first tube, 2 ml of culture was added and the last tube with sterile media (media control). Antibiotic was added to the first tube (containing 2 ml culture) to obtain the maximum concentration that was tested (eg. 25.6 μg/ml for kanamycin), mixed properly, and serially diluted by transferring 1 ml. The tubes were incubated at 37^0C with shaking for ~18 hrs and observed for visible growth to determine MIC. All tests were performed with a minimum of three biological replicates.

Statistical analysis. Statistical analyses were performed using *t* test or multiple unpaired *t* test with Welch correction (with α=0.05) and presented within the text. A minimum of 3 biological replicates were tested.

Data availability. All data are provided within the text.

Acknowledgements

The authors are grateful to J. Wen for primer extension analyses. The authors thank M. Hauser, S. Kauffmann, T. Brandenburg, S. Shore, P. Hwang and A. Fahim for technical assistance. They also thank T. Reynolds and R. D. Johnston for helpful discussions.

Funding

This work was partially supported by grants R15GM106291 (E.M.F) and R01GM120642 (to F.N.B). The content is solely the responsibility of the authors and does not necessarily represent the official views of the National Institutes of Health.

Conflicts of Interest

The authors declare no conflict of interests.

600

601

602 **REFERENCES**

603

604 1. Verstraeten N, Knapen WJ, Kint CI, Liebens V, Van den Bergh B, Dewachter L, Michiels JE, Fu
605 Q, David CC, Fierro AC, Marchal K, Beirlant J, Versées W, Hofkens J, Jansen M, Fauvart M,
606 Michiels J. 2015. Obg and membrane depolarization are part of a microbial bet-hedging strategy
607 that leads to antibiotic tolerance. Mol Cell 59:9–21.
608 2. Hall AM, Gollan B, Helaine S. 2017. Toxin-antitoxin systems: reversible toxicity. Curr Opin
609 Microbiol 36:102–110.
610 3. Aakre CD, Phung TN, Huang D, Laub MT. 2013. A bacterial toxin inhibits DNA replication
611 elongation through a direct interaction with the β sliding clamp. Mol Cell 52:617–628.
612 4. Page R, Peti W. 2016. Toxin-antitoxin systems in bacterial growth arrest and persistence. Nat
613 Chem Biol 12:208–214.
614 5. Van Melderen L, Saavedra De Bast M. 2009. Bacterial toxin-antitoxin systems: more than selfish
615 entities? PLoS Genet 5:e1000437.
616 6. Wang X, Yao J, Sun Y-C, Wood TK. 2021. Type VII toxin/antitoxin classification system for
617 antitoxins that enzymatically neutralize toxins. Trends Microbiol 29:388–393.
618 7. Li M, Gong L, Cheng F, Yu H, Zhao D, Wang R, Wang T, Zhang S, Zhou J, Shmakov SA, Koonin
619 EV, Xiang H. 2021. Toxin-antitoxin RNA pairs safeguard CRISPR-Cas systems. Science 372.
620 8. Ogura T, Hiraga S. 1983. Mini-F plasmid genes that couple host cell division to plasmid
621 proliferation. Proc Natl Acad Sci USA 80:4784–4788.
622 9. Brantl S. 2012. Bacterial type I toxin-antitoxin systems. RNA Biol 9:1488–1490.
623 10. Wen J, Fozo EM. 2014. sRNA antitoxins: more than one way to repress a toxin. Toxins (Basel)
624 6:2310–2335.
625 11. Goormaghtigh F, Fraikin N, Putrinš M, Hallaert T, Hauryliuk V, Garcia-Pino A, Sjödin A,
626 Kasvandik S, Udekwu K, Tenson T, Kaldalu N, Van Melderen L. 2018. Reassessing the role of
627 Type II toxin-antitoxin systems in formation of *Escherichia coli* type II persister cells. MBio 9.
628 12. Andresen L, Martínez-Burgo Y, Nilsson Zangelin J, Rizvanovic A, Holmqvist E. 2020. The small
629 toxic *Salmonella* protein TimP targets the cytoplasmic membrane and is repressed by the small
630 RNA TimR. MBio 11.
631 13. Tsilibaris V, Maenhaut-Michel G, Mine N, Van Melderen L. 2007. What is the benefit to
632 *Escherichia coli* of having multiple toxin-antitoxin systems in its genome? J Bacteriol 189:6101–
633 6108.
634 14. Fozo EM, Makarova KS, Shabalina SA, Yutin N, Koonin EV, Storz G. 2010. Abundance of type I
635 toxin-antitoxin systems in bacteria: searches for new candidates and discovery of novel families.

Nucleic Acids Res 38:3743–3759.
15. Wen J, Won D, Fozo EM. 2014. The ZorO-OrzO type I toxin-antitoxin locus: repression by the OrzO antitoxin. Nucleic Acids Res 42:1930–1946.
16. Unoson C, Wagner EGH. 2008. A small SOS-induced toxin is targeted against the inner membrane in *Escherichia coli*. Mol Microbiol 70:258–270.
17. Wilmaerts D, Bayoumi M, Dewachter L, Knapen W, Mika JT, Hofkens J, Dedecker P, Maglia G, Verstraeten N, Michiels J. 2018. The persistence-inducing toxin HokB forms dynamic pores that cause ATP leakage. MBio 9.
18. Korkut DN, Alves ID, Vogel A, Chabas S, Sharma CM, Martinez D, Loquet A, Salgado GF, Darfeuille F. 2020. Structural insights into the AapA1 toxin of *Helicobacter pylori*. Biochim Biophys Acta Gen Subj 1864:129423.
19. Otsuka Y, Ishikawa T, Takahashi C, Masuda M. 2019. A short peptide derived from the ZorO toxin functions as an effective antimicrobial. Toxins (Basel) 11.
20. Masachis S, Darfeuille F. 2018. Type I toxin-antitoxin systems: regulating toxin expression via Shine-Dalgarno sequence sequestration and small RNA binding. Microbiol Spectr 6.
21. Darfeuille F, Unoson C, Vogel J, Wagner EGH. 2007. An antisense RNA inhibits translation by competing with standby ribosomes. Mol Cell 26:381–392.
22. Wen J, Harp JR, Fozo EM. 2017. The 5′ UTR of the type I toxin ZorO can both inhibit and enhance translation. Nucleic Acids Res 45:4006–4020.
23. Berghoff BA, Hoekzema M, Aulbach L, Wagner EGH. 2017. Two regulatory RNA elements affect TisB-dependent depolarization and persister formation. Mol Microbiol 103:1020–1033.
24. Hemm MR, Paul BJ, Schneider TD, Storz G, Rudd KE. 2008. Small membrane proteins found by comparative genomics and ribosome binding site models. Mol Microbiol 70:1487–1501.
25. Woody RW. 1995. [4] Circular dichroism, p. 34–71. *In* Biochemical Spectroscopy. Elsevier.
26. Bürck J, Wadhwani P, Fanghänel S, Ulrich AS. 2016. Oriented circular dichroism: a method to characterize membrane-active peptides in oriented lipid bilayers. Acc Chem Res 49:184–192.
27. Gurnev PA, Ortenberg R, Dörr T, Lewis K, Bezrukov SM. 2012. Persister-promoting bacterial toxin TisB produces anion-selective pores in planar lipid bilayers. FEBS Lett 586:2529–2534.
28. Weel-Sneve R, Kristiansen KI, Odsbu I, Dalhus B, Booth J, Rognes T, Skarstad K, Bjørås M. 2013. Single transmembrane peptide DinQ modulates membrane-dependent activities. PLoS Genet 9:e1003260.
29. Fozo EM, Kawano M, Fontaine F, Kaya Y, Mendieta KS, Jones KL, Ocampo A, Rudd KE, Storz G. 2008. Repression of small toxic protein synthesis by the Sib and OhsC small RNAs. Mol Microbiol 70:1076–1093.

30. Wickens HJ, Pinney RJ, Mason DJ, Gant VA. 2000. Flow cytometric investigation of filamentation, membrane patency, and membrane potential in *Escherichia coli* following ciprofloxacin exposure. Antimicrob Agents Chemother 44:682–687.
31. Wilmaerts D, Dewachter L, De Loose P-J, Bollen C, Verstraeten N, Michiels J. 2019. HokB monomerization and membrane repolarization control persister awakening. Mol Cell 75:1031–1042.e4.
32. Shan Y, Brown Gandt A, Rowe SE, Deisinger JP, Conlon BP, Lewis K. 2017. ATP-dependent persister formation in *Escherichia coli*. MBio 8.
33. Conlon BP, Rowe SE, Gandt AB, Nuxoll AS, Donegan NP, Zalis EA, Clair G, Adkins JN, Cheung AL, Lewis K. 2016. Persister formation in *Staphylococcus aureus* is associated with ATP depletion. Nat Microbiol 1:16051.
34. Dörr T, Lewis K, Vulić M. 2009. SOS response induces persistence to fluoroquinolones in *Escherichia coli*. PLoS Genet 5:e1000760.
35. Dörr T, Vulić M, Lewis K. 2010. Ciprofloxacin causes persister formation by inducing the TisB toxin in *Escherichia coli*. PLoS Biol 8:e1000317.
36. Schwarz S, Loeffler A, Kadlec K. 2017. Bacterial resistance to antimicrobial agents and its impact on veterinary and human medicine. Vet Dermatol 28:82-e19.
37. Harms A, Brodersen DE, Mitarai N, Gerdes K. 2018. Toxins, targets, and triggers: an overview of toxin-antitoxin biology. Mol Cell 70:768–784.
38. Franch T, Gultyaev AP, Gerdes K. 1997. Programmed cell death by *hok/sok* of plasmid R1: processing at the *hok* mRNA 3'-end triggers structural rearrangements that allow translation and antisense RNA binding. J Mol Biol 273:38–51.
39. Arnion H, Korkut DN, Masachis Gelo S, Chabas S, Reignier J, Iost I, Darfeuille F. 2017. Mechanistic insights into type I toxin antitoxin systems in *Helicobacter pylori*: the importance of mRNA folding in controlling toxin expression. Nucleic Acids Res 45:4782–4795.
40. Romilly C, Deindl S, Wagner EGH. 2019. The ribosomal protein S1-dependent standby site in *tisB* mRNA consists of a single-stranded region and a 5' structure element. Proc Natl Acad Sci USA 116:15901–15906.
41. Kawano M, Reynolds AA, Miranda-Rios J, Storz G. 2005. Detection of 5'- and 3'-UTR-derived small RNAs and cis-encoded antisense RNAs in *Escherichia coli*. Nucleic Acids Res 33:1040–1050.
42. Scott HL, Nguyen VP, Alves DS, Davis FL, Booth KR, Bryner J, Barrera FN. 2015. The negative charge of the membrane has opposite effects on the membrane entry and exit of pH-low insertion peptide. Biochemistry 54:1709–1712.

43. Nguyen VP, Dixson AC, Barrera FN. 2019. The effect of phosphatidylserine on a pH-responsive peptide is defined by its noninserting end. Biophys J 117:659–667.
44. Nguyen VP, Alves DS, Scott HL, Davis FL, Barrera FN. 2015. A novel soluble peptide with pH-responsive membrane insertion. Biochemistry 54:6567–6575.
45. Sayed N, Nonin-Lecomte S, Réty S, Felden B. 2012. Functional and structural insights of a *Staphylococcus aureus* apoptotic-like membrane peptide from a toxin-antitoxin module. J Biol Chem 287:43454–43463.
46. El Mortaji L, Tejada-Arranz A, Rifflet A, Boneca IG, Pehau-Arnaudet G, Radicella JP, Marsin S, De Reuse H. 2020. A peptide of a type I toxin-antitoxin system induces *Helicobacter pylori* morphological transformation from spiral shape to coccoids. Proc Natl Acad Sci USA 117:31398–31409.
47. Weaver KE, Weaver DM, Wells CL, Waters CM, Gardner ME, Ehli EA. 2003. *Enterococcus faecalis* plasmid pAD1-encoded Fst toxin affects membrane permeability and alters cellular responses to lantibiotics. J Bacteriol 185:2169–2177.
48. Kawano M, Oshima T, Kasai H, Mori H. 2002. Molecular characterization of long direct repeat (LDR) sequences expressing a stable mRNA encoding for a 35-amino-acid cell-killing peptide and a cis-encoded small antisense RNA in *Escherichia coli*. Mol Microbiol 45:333–349.
49. Jahn N, Brantl S, Strahl H. 2015. Against the mainstream: the membrane-associated type I toxin BsrG from *Bacillus subtilis* interferes with cell envelope biosynthesis without increasing membrane permeability. Mol Microbiol 98:651–666.
50. Gerdes K, Rasmussen PB, Molin S. 1986. Unique type of plasmid maintenance function: postsegregational killing of plasmid-free cells. Proc Natl Acad Sci USA 83:3116–3120.
51. Patel S, Weaver KE. 2006. Addiction toxin Fst has unique effects on chromosome segregation and cell division in *Enterococcus faecalis* and *Bacillus subtilis*. J Bacteriol 188:5374–5384.
52. Weaver KE, Reddy SG, Brinkman CL, Patel S, Bayles KW, Endres JL. 2009. Identification and characterization of a family of toxin-antitoxin systems related to the *Enterococcus faecalis* plasmid pAD1 *par* addiction module. Microbiology (Reading, Engl) 155:2930–2940.
53. Knopp M, Gudmundsdottir JS, Nilsson T, König F, Warsi O, Rajer F, Ädelroth P, Andersson DI. 2019. *De novo* emergence of peptides that confer antibiotic resistance. MBio 10.
54. Schneider V, Wadhwani P, Reichert J, Bürck J, Elstner M, Ulrich AS, Kubař T. 2019. Tetrameric charge-aipper assembly of the TisB peptide in membranes-computer simulation and experiment. J Phys Chem B 123:1770–1779.
55. 2019. Bacterial resistance to antibiotics – from molecules to man. Wiley.
56. Bolivar F, Rodriguez RL, Greene PJ, Betlach MC, Heyneker HL, Boyer HW, Crosa JH, Falkow S.

1977. Construction and characterization of new cloning vehicles. II. A multipurpose cloning system. Gene 2:95–113.

57. Fontaine F, Fuchs RT, Storz G. 2011. Membrane localization of small proteins in *Escherichia coli*. J Biol Chem 286:32464–32474.

58. Cherepanov PP, Wackernagel W. 1995. Gene disruption in *Escherichia coli*: Tc^R and Km^R cassettes with the option of Flp-catalyzed excision of the antibiotic-resistance determinant. Gene 158:9–14.

59. Murphy KC, Campellone KG. 2003. Lambda Red-mediated recombinogenic engineering of enterohemorrhagic and enteropathogenic *E. coli*. BMC Mol Biol 4:11.

60. Datsenko KA, Wanner BL. 2000. One-step inactivation of chromosomal genes in *Escherichia coli* K-12 using PCR products. Proc Natl Acad Sci USA 97:6640–6645.

61. Doublet B, Douard G, Targant H, Meunier D, Madec J-Y, Cloeckaert A. 2008. Antibiotic marker modifications of lambda red and FLP helper plasmids, pKD46 and pCP20, for inactivation of chromosomal genes using PCR products in multidrug-resistant strains. J Microbiol Methods 75:359–361.

62. Massé E, Escorcia FE, Gottesman S. 2003. Coupled degradation of a small regulatory RNA and its mRNA targets in *Escherichia coli*. Genes Dev 17:2374–2383.

63. Opdyke JA, Kang J-G, Storz G. 2004. GadY, a small-RNA regulator of acid response genes in *Escherichia coli*. J Bacteriol 186:6698–6705.

64. Hemm MR, Paul BJ, Miranda-Ríos J, Zhang A, Soltanzad N, Storz G. 2010. Small stress response proteins in *Escherichia coli*: proteins missed by classical proteomic studies. J Bacteriol 192:46–58.

65. Usery RD, Enoki TA, Wickramasinghe SP, Nguyen VP, Ackerman DG, Greathouse DV, Koeppe RE, Barrera FN, Feigenson GW. 2018. Membrane bending moduli of coexisting liquid phases containing transmembrane peptide. Biophys J 114:2152–2164.

66. Alves DS, Westerfield JM, Shi X, Nguyen VP, Stefanski KM, Booth KR, Kim S, Morrell-Falvey J, Wang B-C, Abel SM, Smith AW, Barrera FN. 2018. A novel pH-dependent membrane peptide that binds to EphA2 and inhibits cell migration. Elife 7.

67. Schneider CA, Rasband WS, Eliceiri KW. 2012. NIH Image to ImageJ: 25 years of image analysis. Nat Methods 9:671–675.

68. 2003. Determination of minimum inhibitory concentrations (MICs) of antibacterial agents by broth dilution. Clin Microbiol Infect 9:ix–xv.

FIGURE LEGENDS

FIG 1 The 5'UTR variant of *zorO* gene and its effect on growth, survival and translation. Schematic of the full-length (174 nts; P_{BAD}-*zorO*-FLAG) and processed (Δ28; P_{BAD}-Δ28*zorO*-FLAG) UTR of *zorO* used in the study (A). Growth curve of MG1655 derived cells (UTK007) carrying respective plasmids after induction with arabinose concentration of 13.32 mM (B), 6.67 μM (C) and 0.67 μM (D) during mid-log phase (B-D, *n*=3, shown are mean ± standard deviation [SD]). Log survival (colony forming units) of cells after ZorO overproduction with indicated arabinose concentrations (E) (*n*=9, shown are mean ± SD). Dot blot assay after 30 min with 13.32 mM arabinose induction of FLAG tagged ZorO in *E. coli* UTK 007 cells from the two 5' UTR variants (10 μg and 20 μg of total protein loaded) (F); pAZ3- negative control, PC- positive control (No-UTR-FLAG-*zorO*).

FIG 2 Synthetic ZorO peptide can insert across a lipid bilayer. Circular dichroism spectra of ZorO peptide in lipid composition partially mimicking *E. coli* membrane (A). Oriented circular dichroism of ZorO peptide on lipid bilayer (B).

FIG 3 ZorO overproduction leads to membrane depolarization and ATP depletion. Cells overproducing ZorO under the control of the two 5' UTR variants; 15 and 30 min post-induction were analyzed via flow-cytometry after staining with $DiBAC_4$-3. Bar graphs quantifying percent of depolarized cells with 1.33 μM (A) and 3.33 μM (B) arabinose concentration ($n \geq 5$). Relative ATP levels after ZorO overexpression from respective 5'UTRs and arabinose induction after 15 min (C) and 30 min (D) (*n*=3). For all panels shown are mean ± SD. The *p* values were calculated using a multiple unpaired *t* test with Welch correction (ns, not significant, *, $p < 0.05$, **, $p < 0.01$, ***, $p < 0.001$).

FIG 4 ZorO overproduction does not lead to gross alterations of cellular morphology. Scanning electron microgram of *E. coli* cells overproducing ZorO from P_{BAD}-No-UTR-*zorO* plasmids with 13.32 mM arabinose induction for 30 min (A) compared to that of uninduced cells (B); right panels 20000X and left panels 5000X magnification. Comparison of cell length after ZorO overproduction. Shown are mean ± SD. The *p* values were calculated using *t* test with Welch correction (****, $p < 0.0001$).

FIG 5 Multiple copies of the *zor-orz* locus allows for growth in the presence of kanamycin in MG1655. Growth curve of *E. coli* UTK007 harboring pBR322 (black) or pBR-*zor-orz* (turquoise) in LB (A), LB with 4μg/mL kanamycin (B), M9 minimal media with 0.2% glucose (C), M9 minimal media with 0.2% glucose and 4 μg/mL kanamycin (D), M9 minimal media with 0.4% fructose (E), and M9 minimal media with 0.4% fructose and 4 μg/mL kanamycin (F). $n \geq 9$; shown are mean ± SD. All growth conditions contained 100 μg/mL ampicillin for plasmid maintenance.

FIG 6 Multiple copies of the *zor-orz* locus allows for growth in the presence of kanamycin in EDL933 Growth curve of EDL-Δ*zor-orz* harboring pBR322 (black) or pBR-*zor-orz* (turquoise) in LB (A), LB with 8 μg/mL kanamycin (B), in M9 minimal media with 0.2% glucose (C), M9 minimal media with 0.2% glucose and 4 μg/mL kanamycin (D) or M9 minimal media with 0.4% fructose (E), and M9 minimal media with 0.4% fructose and 4 μg/mL kanamycin (F). All growth conditions contained 100 μg/mL ampicillin for plasmid maintenance. $n \geq 3$, shown are mean ± SD.

FIG 7 A single chromosomal copy of processed 5'UTR-*zorO* does not improve growth in the presence of aminoglycosides. Growth curve of MG1655 strains carrying *zorO* with a processed 5' UTR (turquoise) compared to the wild type MG1655 in LB (A), LB with 4 μg/mL kanamycin (B) and LB with 4 μg/mL gentamicin (C). Growth curve of WT EDL933 (black) compared to that of the EDL933-Δ*zor-orz* (turquoise) and EDL933-Δ28-*zorO* (salmon) in LB (D), LB with 8 μg/mL kanamycin (E) and LB with 4 μg/mL gentamycin (F). For all panels n=3; shown are mean ± SD.

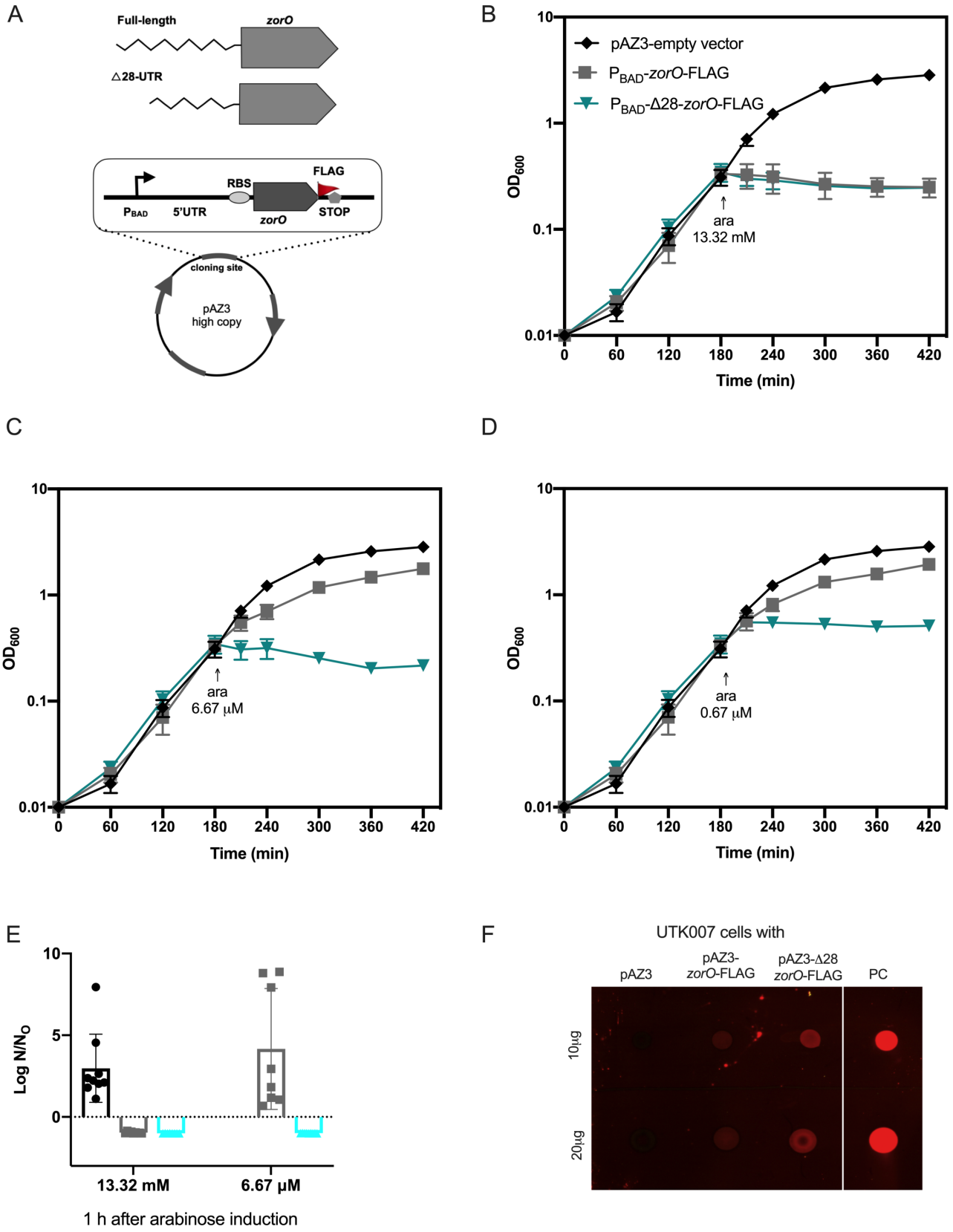

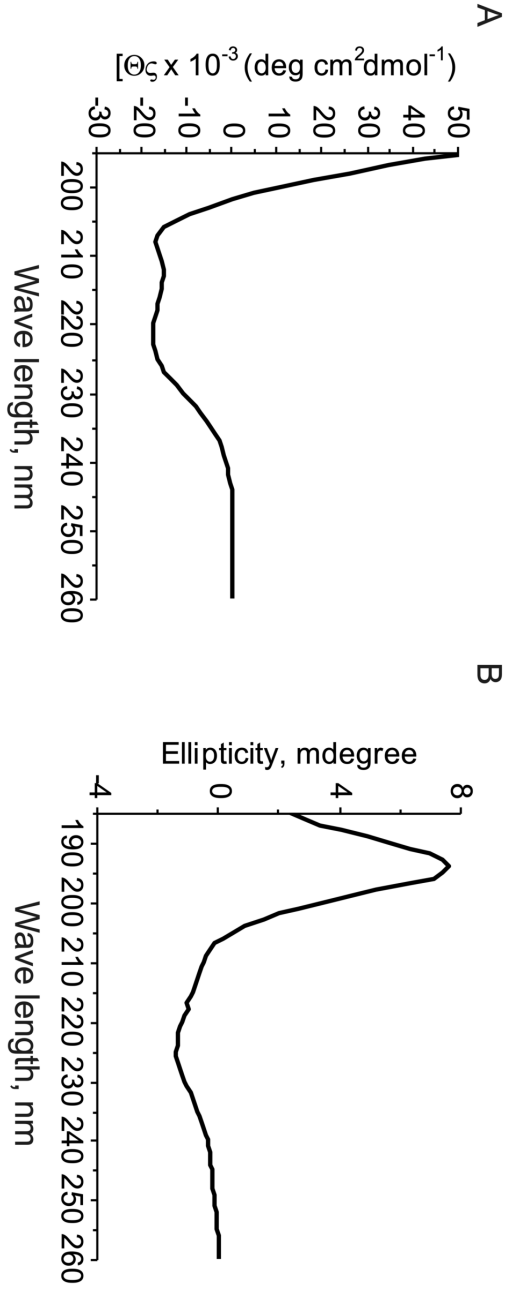

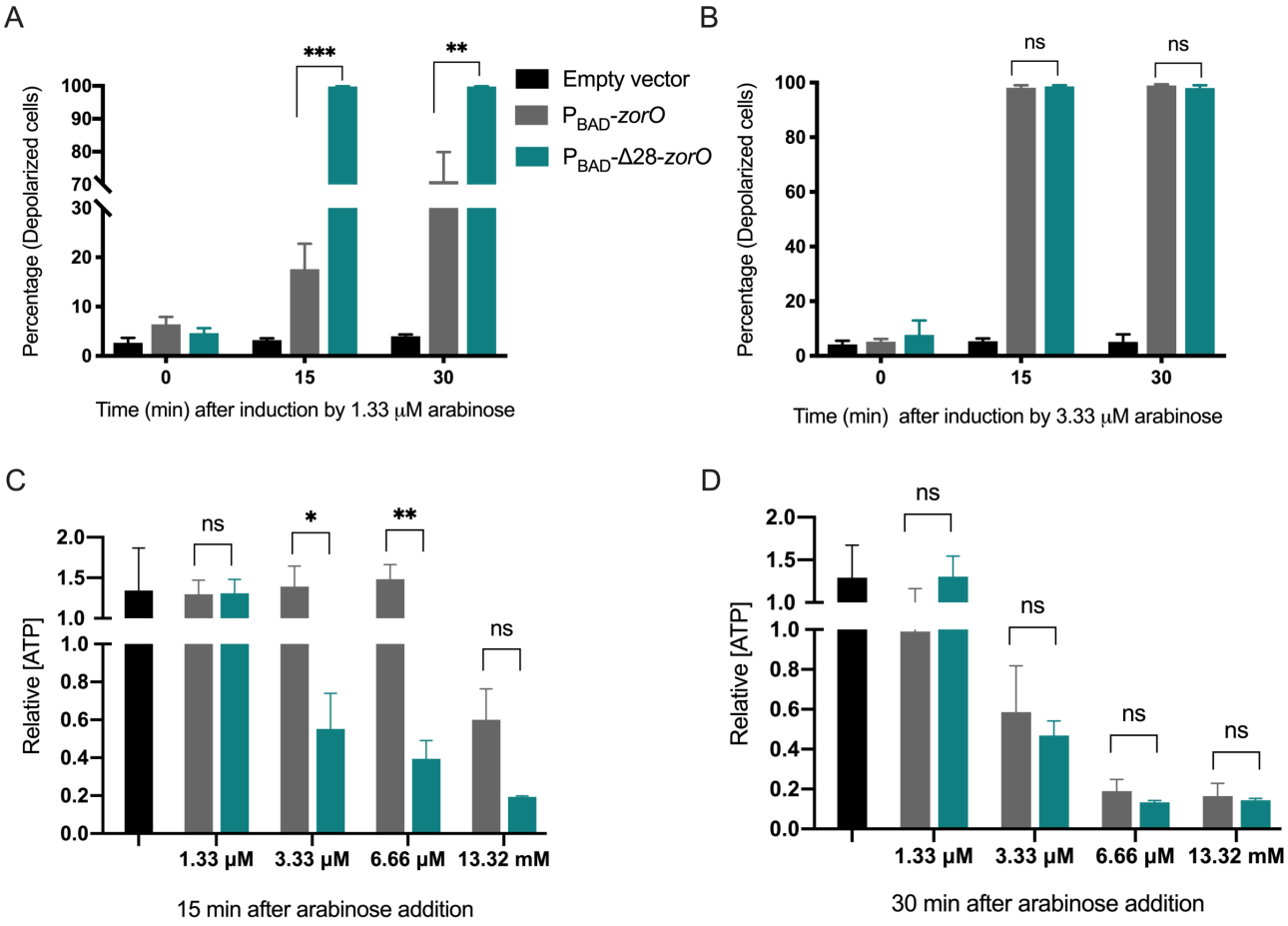

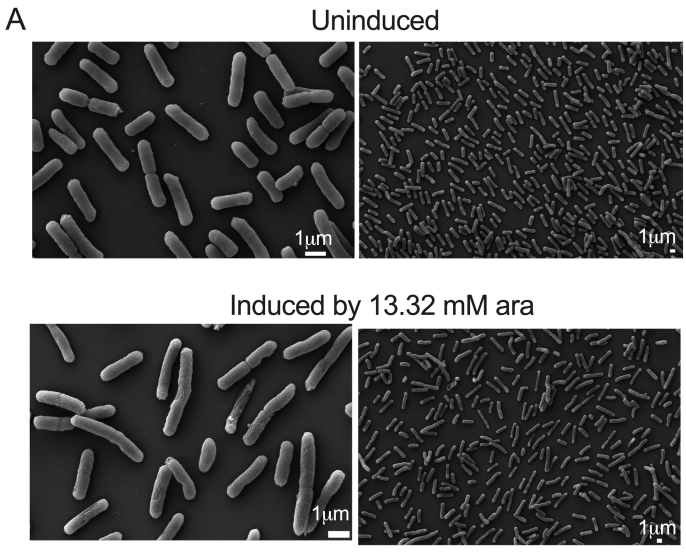

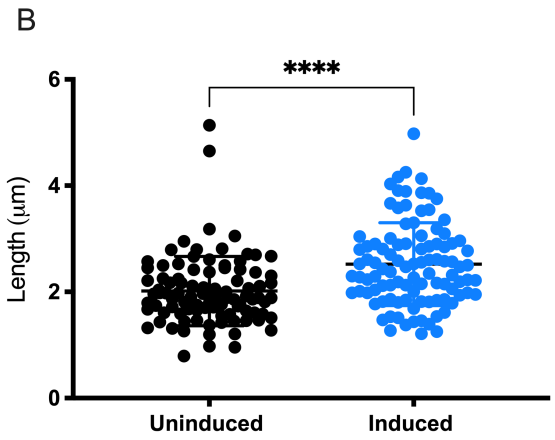

Journal of Bacteriology

JB

Journal of Bacteriology

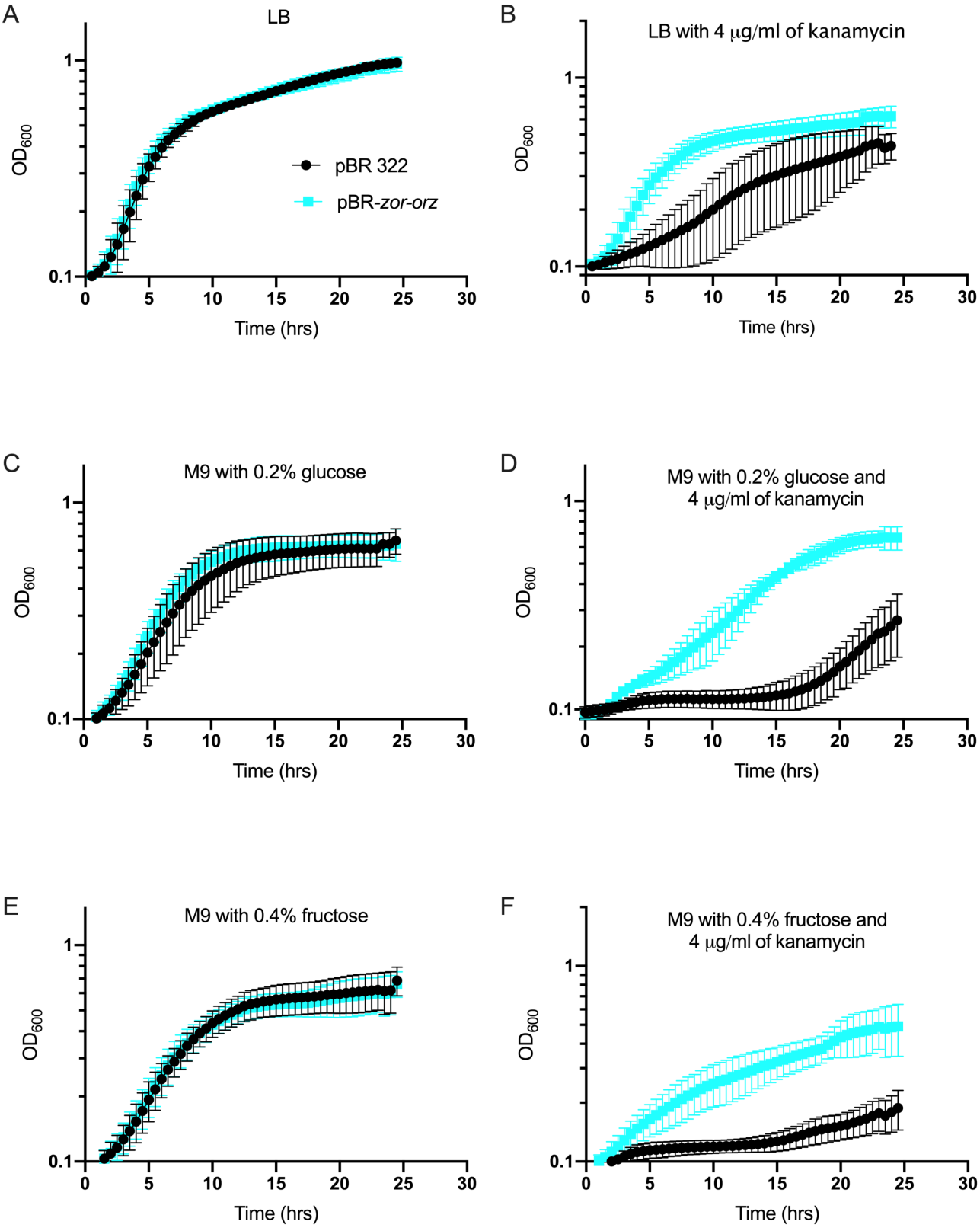

Journal of Bacteriology

JB

Journal of Bacteriology